Structure, stability, and electronic properties of $SrTiO_3/LaAlO_3$ and $SrTiO_3/SrRuO_3$ interfaces

J.-M. Albina,[1,2] M. Mrovec,[1,2] B. Meyer,[3] and C. Elsässer[1,2]
[1]*Fraunhofer Institute for Mechanics of Materials IWM, Wöhlerstrasse 11, 79108 Freiburg, Germany*
[2]*IZBS, University of Karlsruhe, Kaiserstrasse 12, 76131 Karlsruhe, Germany*
[3]*Chair for Theoretical Chemistry, Ruhr-University Bochum, 44780 Bochum, Germany*
(Received 21 May 2007; revised manuscript received 23 July 2007; published 1 October 2007)

Density functional theory by means of the mixed-basis pseudopotential method was employed to carry out electronic-structure calculations of interfaces in $SrTiO_3/LaAlO_3$ and $SrTiO_3/SrRuO_3$ perovskite heterophase systems. The main objective of the work is to investigate the influence of different structural and chemical terminations of the interfaces on their electronic and adhesive properties. The investigated supercells therefore include not only interfaces with a regular perovskite stacking but also interfaces with planar stacking-fault-like defects of Ruddlesden-Popper and Magneli types. Stability of interfaces is assessed by calculating rigid and relaxed works of separation. Band offsets and Schottky barriers are determined for the insulator/insulator $SrTiO_3/LaAlO_3$ and the insulator/conductor $SrTiO_3/SrRuO_3$ systems, respectively.

DOI: 10.1103/PhysRevB.76.165103 PACS number(s): 71.15.−m, 73.30.+y, 73.40.Qv, 77.55.+f

I. INTRODUCTION

Devices made of dielectric and ferroelectric oxides with the ABO_3 perovskite crystal structure have attracted considerable interest from the electronics industry.[1,2] Currently, perovskite oxides are used in numerous applications including sensors in infrared cameras, piezoelectric actuators and transducers, and even microelectromechanical systems in airbag accelerometers. However, the most exciting and economically important is the use of perovskite oxides in integrated microelectronic devices, for example, as capacitors in nonvolatile ferroelectric or dynamic random access memories or as the gate insulators in the next generation of field-effect transistor devices.[3–5]

These modern integrated microelectronic components require the stacking sequence of different metallic and insulating thin films in order to reach the targeted performance and reliability. Due to progressing miniaturization, the key attributes, e.g., dielectric capacitance or ferroelectric polarization, high thermal stability, and low leakage current, however, depend not only on intrinsic properties of the bulk or thin-film materials but also on the interfaces between them.

The understanding and control of the interfaces are critical for the integration and fabrication of reliable perovskite heterostructures.[6] Many of the unique functional properties of perovskites may be enhanced but also destroyed by local stresses and strains or by structural imperfections, such as bulk and interface dislocations, planar stacking faults, and grain boundaries. On the other hand, perovskite heterostructures with a small lattice mismatch can be grown epitaxially without bulk dislocations or grain boundaries. Such atomically sharp interfaces can be studied nowadays with high precision using accurate *ab initio* methods.

In this work, we performed first-principles electronic-structure calculations of two model perovskite heterostructure systems in order to investigate the influence of the interfacial structure on electronic and adhesive properties. The two investigated systems, $SrTiO_3/LaAlO_3$ (001) (STO/LAO) and $SrTiO_3/SrRuO_3$ (001) (STO/SRO), were chosen as representative models of insulator/insulator (or substrate/dielectric) and insulator/conductor (or dielectric/electrode) perovskite contacts, respectively.

A recent discovery[7] of remarkable electrical properties of interfaces in the STO/LAO system has attracted considerable attention from several research groups.[8–14] A series of experiments has confirmed an existence of not only an insulating but also a highly conducting interface between the two insulating perovskites. It was found that the interfacial termination of LAO is the critical parameter: while the LaO-terminated interface is electrically insulating, the AlO_2-terminated interface turns out to be conducting. The debate about the extent to which the observed behavior is intrinsic to the system and about the influence of other factors, such as the role oxygen vacancies, preparation conditions, interface roughening, and electrical fields, is still ongoing. Apart from these striking discoveries, (001)-oriented LAO crystal surfaces are often used as substrates for the epitaxial growth of dielectric STO and other perovskites. A small lattice mismatch of 3% between the STO and LAO perovskites allows the coherent growth of STO films on LAO substrates by pulsed-laser deposition. Above a critical film thickness, misfit dislocations with Burgers vectors $a\langle 100\rangle$ and $a\langle 110\rangle$ are observed to form in STO. These defects are, however, well separated and the interface between them is coherent and atomically flat.[15]

While the STO/LAO system is a hot topic in the experimental community, to our knowledge, only few theoretical studies are available.[16–18] In a recent study, Gemming and Seifert[16] have focused on structural, electronic and dielectric properties of STO/LAO multilayers. The electrical behavior of the STO/LAO interfaces was investigated by Pentcheva and Pickett[17] and by Park *et al.*[18] but neither of these studies was able to provide a complete explanation of the astonishing electrical properties.

The STO/SRO heterophase interface system is a prototype of a conducting electrode film deposited on an insulating dielectric substrate. Due to its good electrical conductivity, high thermal and chemical stabilities, and good lattice matching with other oxides, SRO is often used for contact electrodes in electroceramic devices. A small lattice mis-

match of only 0.64% allows the growth of high-quality films of SRO on STO with smooth surfaces and atomically sharp interfaces.[19–21] The in-plane orientation relation of these epitaxial heterostructures is SRO[$\bar{1}$10]‖STO[010] and SRO[001]‖STO[100].[22] Furthermore, a possible application of a broad variety of deposition methods, e.g., pulsed-laser deposition,[19] metal-organic chemical vapor deposition, rf magnetron, or 90° off-axis sputtering, makes SRO a flexible material for research purposes. There also exists an extensive number of experimental studies of SRO thin films and their interfaces with other materials.[19–27]

The aim of the present paper is to obtain information about band offsets and Schottky barriers and mechanical stabilities of interfaces in the SRO/STO and STO/LAO systems. A reliable determination of these properties is a necessary requirement for a successful design of perovskite-based heterostructures. Since hardly any experimental measurements of such barriers in epitaxial perovskite heterostructures have been reported, it is useful to have a theoretical approach complementary to the experiment for evaluating these electronic properties in heterophase systems.

The paper is organized as follows. Section II covers computational details of our performed calculations and gives an overview of investigated systems. In Sec. III, the computed results of structural, mechanical, and electronic properties of both bulk and heterostructure systems are presented and the influence of different interfacial terminations is analyzed. A summary of the work is given in Sec. IV.

II. COMPUTATIONAL METHOD AND STRUCTURE MODELS

A. Mixed-basis pseudopotential method

The electronic-structure calculations of heterophase interfaces were performed within the density functional theory (DFT) framework.[28,29] The Kohn-Sham equations were solved by means of a mixed-basis pseudopotential approach.[30–34] The local density approximation (LDA) was used for exchange and correlation.[35,36] Interactions between ionic cores and valence electrons were treated by norm-conserving nonlocal ionic pseudopotentials.[37] Pseudopotentials were generated from neutral atoms with the following electronic configurations: for O[He] $2s^2 2p^{3.50} 3d^{0.50}$, for Al[Ne] $3s^2 3p^{0.70} 3d^{0.30}$, and for Ru[Kr] $5s^{0.25} 5p^{0.25} 4d^{7.50}$. Ionic reference configurations of the pseudopotentials were set for La^{3+}([Kr] $5s^2 5p^6$), Sr^{2+}([Ar] $4s^2 4p^6$), and Ti^{4+}([Ne] $3s^2 3p^6$). Localized functions were employed in addition to plane waves in the mixed basis to represent O $2p$ valence states, Ti $3s$ and $3p$ semicore and $3d$ valence states, Ru $4d$ valence states, Sr $4s$ and $4p$ semicore states, and La $5s$ and $5p$ semicore and $5d$ valence states. These localized orbitals were confined within the following sphere radii: $r_{lo}(\mathrm{Sr}) = r_{lo}(\mathrm{La}) = r_{lo}(\mathrm{O}) = 1.9$ a.u. and $r_{lo}(\mathrm{Ti}) = r_{lo}(\mathrm{Ru}) = 1.6$ a.u.

Bulk properties of the perovskites were calculated with up to $(6\times6\times6)$ Monkhorst-Pack[38] k-point meshes for the insulating STO and LAO, and $(16\times16\times16)$ for the conductive SRO. The cutoff energy of the plane waves used in the mixed basis was set up to 25 Ry. For calculations of the electronic energy barriers and the works of separation for the heterostructures, a $(4\times4\times1)$ k-point mesh and the plane wave cutoff of 15 Ry were determined to be sufficient for well converged results.

Local electronic structures were analyzed by site-projected electronic densities of states (DOSs) at oxygen atoms. A sphere radius of $r_{pr}(O^{2-}) = 2.84$ a.u. was chosen to enclose the formal ionic charge of the oxygen ion in this projection sphere for the DOS. Gaussian broadening with the width of 0.2 eV was applied for plotting the DOS and reduced to 0.1 eV for accurate determination of valence band edges.

B. Crystal structures of bulk perovskites

Bulk $SrTiO_3$ is a typical representative of the perovskite family. It crystallizes at room temperature in a cubic perovskite structure with the lattice constant $a = 3.905$ Å.[39] $LaAlO_3$ and $SrRuO_3$ are perovskites with slight distortions of the BO_6 octahedra from the cubic arrangement at room temperature. However, since the distortions are small, they can be well approximated as pseudocubic structures. The rhombohedral crystal structure of $LaAlO_3$ can then be described as a pseudocubic structure with the lattice parameter $a = 3.790$ Å,[40] while for the orthorhombic crystal structure (lattice parameters $a = 5.5670$ Å, $b = 5.5304$ Å, and $c = 7.8446$ Å) (Ref. 41) of ferromagnetic $SrRuO_3$, the pseudocubic lattice parameter $a = 3.930$ Å.[22]

C. Supercell models of the heterophase interfaces

For all calculations of the perovskite/perovskite interfaces, supercells with three-dimensional periodic boundary conditions were used. The supercells of the heterostructures were composed of seven or nine alternating (002) atomic layers of SrO and TiO_2 for the STO slab and seven or nine alternating atomic layers of either LaO and AlO_2 for the LAO slab, or SrO and RuO_2 for the SRO slab, respectively. The odd number of planes ensures that the two interfaces in the supercells are equivalent and prevents thus the formation of artificial electrostatic fields (we will discuss this issue in more detail in Sec. III C). Each supercell contained only one perovskite unit-cell period in the directions parallel to the interface, which restricts more complex symmetry breaking relaxations and reconstructions. For all supercells, the lateral lattice constant in the x and y directions, i.e., parallel to the interface plane, was fixed equal to the theoretical equilibrium bulk lattice parameter of STO [$a_{STO} = 3.845$ Å (Ref. 42)]. We therefore consider the heterostructures as pseudomorphic systems with a rigid STO substrate. Perpendicular to the interface, in the vertical z direction, the supercell parameter was optimized by total-energy minimization.

Since the supercells are composed of alternating atomic planes with either AO or BO_2 compositions, several variants of interfaces can be formed. For the STO/LAO system, there are two possible terminations for each perovskite, namely, the SrO or TiO_2 termination for STO and the LaO or AlO_2 termination for LAO. Consequently, four distinct contacts

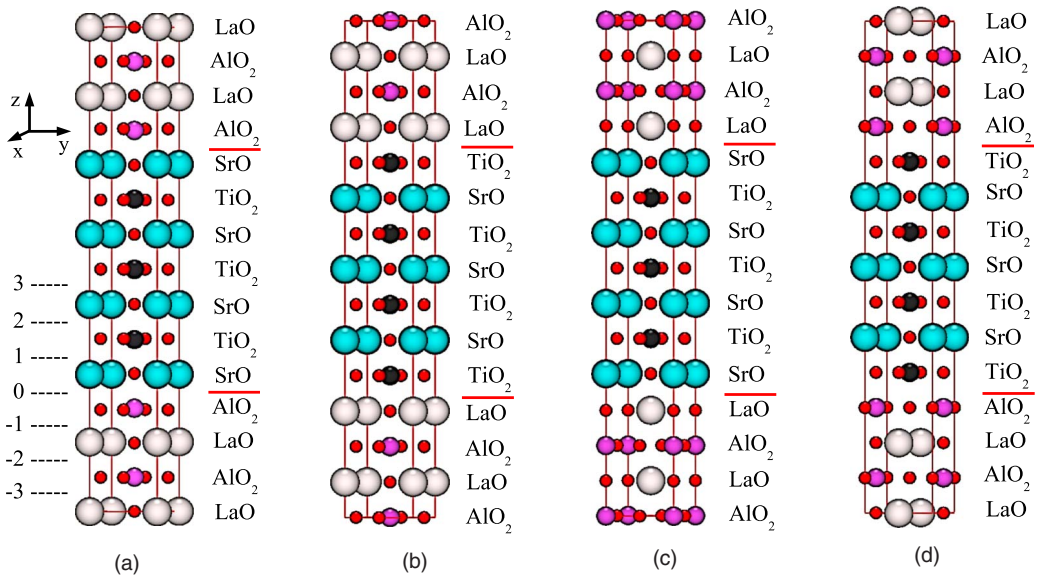

FIG. 1. (Color online) Supercell models of the STO/LAO heterophase interfaces with four possible interface terminations: (a) SrO-AlO_2, (b) LaO-TiO_2, (c) SrO-LaO (Ruddlesden-Popper-type defect), and (d) TiO_2-AlO_2 (Magneli-type defect). Indices are for pair of two adjacent planes (see Fig. 3).

can be built in this heterostructure, which are illustrated in Fig. 1. The first two variants are contacts in which interfaces do not disturb the regular stacking of the AO and BO_2 perovskite layers. This occurs when the SrO termination of STO faces the AlO_2 termination of LAO (SrO-AlO_2) [Fig. 1(a)] or, vice versa, when the TiO_2 termination of STO faces the LaO termination of the LAO (TiO_2-LaO) [Fig. 1(b)]. In the other two possible contacts, the regular alternating stacking is disrupted by stacking-fault-like planar defects created at the interface. The first case, when the SrO termination of STO and the LaO termination of LAO are in contact (SrO-LaO) [Fig. 1(c)], is known as a Ruddlesden-Popper-type defect.[43] This fault is a rather frequent planar defect in perovskite oxides and has been observed both in bulk perovskites[44] and at perovskite interfaces.[26,45] The second type of interface with broken stacking in which the TiO_2 layer from STO faces the AlO_2 layer from LAO (TiO_2-AlO_2) termination) [Fig. 1(d)] can be considered as a Magneli-type defect[46] after a related structural motif found in binary titanium or vanadium oxides.

For the STO/SRO heterostructure, the AO sublattice is common to both perovskites and therefore only three supercells can be discriminated (see Fig. 2). In the defect-free case (a), no distinction can be made between supercells with the TiO_2-SrO and SrO-RuO_2 terminations because the SrO layer can be considered as belonging to both the STO and SRO slabs. The supercell in Fig. 2(a) therefore effectively contains both these interfaces. This degeneracy requires some caution when analyzing properties of this heterostructure. While for some properties (e.g., the rigid work of separation) unique

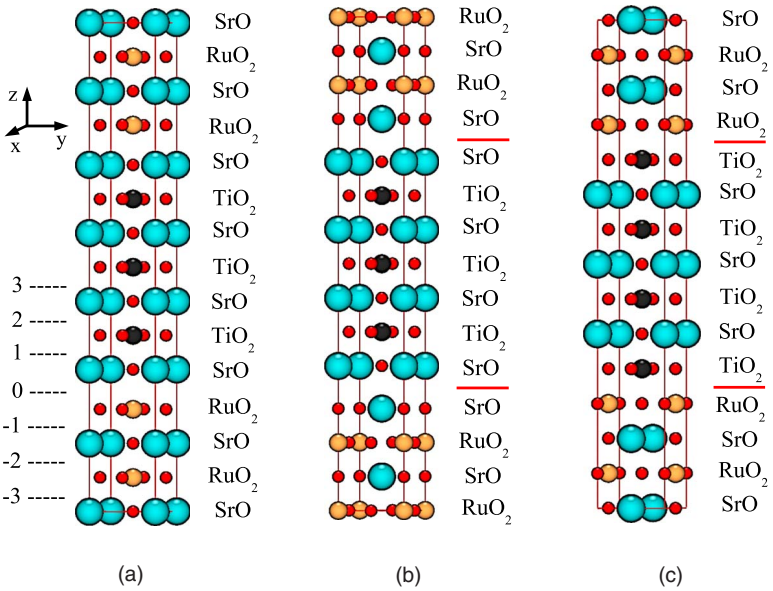

FIG. 2. (Color online) Supercell models of the STO/SRO heterophase interfaces with three possible interface terminations: (a) TiO_2-SrO or SrO-RuO_2, (b) SrO-SrO (Ruddlesden-Popper-type defect), and (c) TiO_2-RuO_2 (Magneli-type defect). Indices are for pair of two adjacent planes (see Fig. 4).

TABLE I. Calculated equilibrium lattice parameter a_0, bulk modulus B_0, and magnetic moment μ_0 of $SrTiO_3$, $LaAlO_3$, and $SrRuO_3$ bulk cubic perovskite phases.

	a_0 (Å)	B_0 (GPa)	μ_0 (μ_B)
$SrTiO_3$	3.845	205	
	3.903[a] (expt.)	183	
$LaAlO_3$	3.739	219	
	3.790[b] (expt.)		
	3.752[c] (calc.)		
$SrRuO_3$ (LDA)	3.923	208	
$SrRuO_3$ (LSDA)	3.927	201	1.167
	3.930[d] (expt.)		1.0–1.55[e]
	3.923[e] (calc.)		1.17[e], 1.73[f]

[a]Reference 50.
[b]Reference 40.
[c]Reference 16.
[d]Reference 41.
[e]Reference 49.
[f]Reference 51.

and well defined values can be obtained for each interface, other quantities (e.g., the electronic properties) correspond to the whole system without the possibility of partitioning into individual contributions from each interface. The Ruddlesden-Popper- and Magneli-type defects correspond in this system to the SrO-SrO (Ref. 24) [Fig. 2(b)] and TiO_2-RuO_2 [Fig. 2(c)] interface terminations, respectively.

One additional complication arises due to different formal charge states of the atomic (002) layers in the three investigated perovskites. The SrO $(Sr^{2+}O^{2-})^0$, TiO_2 $[Ti^{4+}(O^{2-})_2]^0$, and RuO_2 $[Ru^{4+}(O^{2-})_2]^0$ layers are formally charge neutral and the charge neutrality is therefore respected for all STO/SRO supercells. However, in the case of LAO, the AlO_2 layer has formally an excess of one electron $[Al^{3+}(O^{2-})_2]^{1-}$, whereas the LaO layer has a deficiency of one electron $(La^{3+}O^{2-})^{1+}$. Consequently, the STO/LAO supercells have a formal excess of one electron if the LAO slab is AlO_2 terminated (i.e., for the SrO-AlO_2 and TiO_2-AlO_2 interfaces) and a formal deficiency of one electron if the LAO slab is LaO terminated (i.e., for the TiO_2-LaO and SrO-LaO interfaces). In order to compensate for this imbalance, a constant negative or positive background charge density was added in the calculations.

Finally, when investigating polar systems, such as the LAO/STO interface, it is necessary to consider the possible presence of net interface charges (monopole moments[47,48]) and resulting nonzero electrical fields. In most of our calculations, we employed symmetrical although nonstoichiometric supercell configurations with two equivalent interfaces to avoid finite internal electrical fields. Asymmetrical supercell configurations containing a pair of different interfaces, which were used in Ref. 16, consist of stoichiometric, charge neutral perovskites with the same number of AO and BO_2 planes and do not need the compensating charge background. The presence of two different interfaces, however, leads to internal electrical fields and band bendings across the thin films that complicate the determination of band offsets.

TABLE II. Rigid and relaxed works of separation (in J/m^2); values in parentheses are from Ref. 16.

	W_{sep}^{rigid}	$W_{sep}^{relaxed}$
STO		
TiO_2-SrO	3.13	2.71
SrO-SrO	1.78	1.77
TiO_2-TiO_2	1.99	2.10
LAO		
AlO_2-LaO	5.47	5.23
SRO		
RuO_2-SrO	2.70	2.32
STO/LAO		
SrO-AlO_2	3.09 (4.0)	2.84 (3.6)
TiO_2-LaO	3.86 (4.2)	3.62 (3.7)
SrO-LaO	2.17	2.34
TiO_2-AlO_2	2.01	2.21
STO/SRO		
SrO-RuO_2	2.94	2.62
TiO_2-SrO	3.18	2.71
SrO-SrO	1.83	1.78
TiO_2-RuO_2	2.36	2.22

III. RESULTS AND DISCUSSION

A. Bulk properties

As a first step, we calculated cohesive properties of bulk cubic LAO and SRO crystals, namely, their equilibrium lattice constant and bulk modulus. The results are compared to available literature data in Table I. For LAO, the discrepancy between the experimental and the theoretical lattice constant calculated in the present work is less than 2%. The calculated lattice constant for SRO is very close to the experimental value and agrees also well with another theoretical value obtained using the linearized-augmented-plane-wave method.[49] Table I also contains equilibrium properties of cubic STO calculated previously by means of the mixed-basis pseudopotential method.[42]

As already mentioned in the previous section, all calculations of the heterostructure systems were done with the lateral x and y dimensions of the supercell fixed to the theoretical bulk STO lattice parameter. We therefore also determined the minimum energy configurations of strained tetragonal unit cells of LAO and SRO with the lattice parameter a fixed to STO. Due to a smaller cubic lattice parameter than STO, the tetragonal unit cell of LAO exhibits a contraction in the z direction with the c/a ratio of 0.96. An inverse response is found for SRO that undergoes an expansion with the c/a ratio of 1.05.

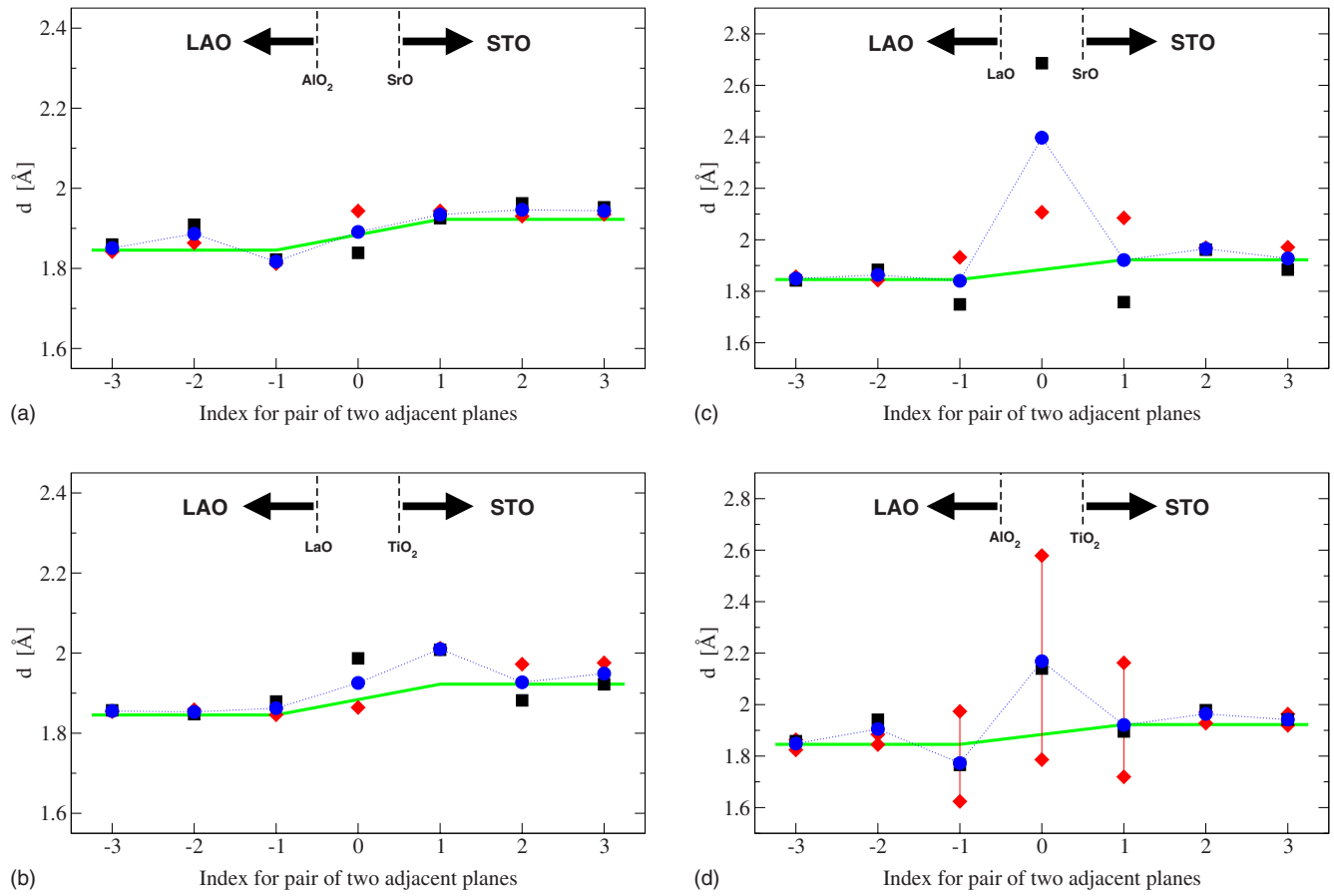

FIG. 3. (Color online) Interplanar spacings along the c axis in the four STO/LAO heterostructures. The graphs [(a)–(d)] correspond to the supercell models [(a)–(d)] of Fig. 1, respectively. Thick solid lines mark ideal bulk spacings in the perovskites. Symbols are DFT results from relaxed supercells, which are marked as follows. Squares, cation-cation interplanar distance; diamonds, oxygen-oxygen interplanar distance; circles connected by dotted lines, average interplanar distance. For the TiO_2-AlO_2 interface in panel (d), two diamonds connected by vertical thin solid lines for each plane indicate two nonequivalent oxygen atoms.

Since SRO is a ferromagnetic perovskite with $T_C = 160$ K,[52] the cubic SRO is more stable in the ferromagnetic state than in the nonmagnetic state.[51] We carried out calculations of bulk properties of magnetic cubic SRO within the local spin density approximation (LSDA) in order to estimate the influence of magnetism. As reported in Table I, no significant changes were found for cohesive properties. The difference in the lattice parameter is less than 1%, and the bulk modulus is less than 4% higher in the LSDA state than in the LDA state. The calculated total magnetic moment of SRO at the equilibrium volume agrees also well with results of LSDA calculations by Singh[49] with the full-potential LAPW method and lies within the range of experimental values. Santi and Jarlborg[51] reported a significantly higher value, which is probably a result of the atomic-sphere approximation in the LMTO method they used.

B. Interfacial stabilities

The stability of interfaces can be estimated by calculating their work of separation. The ideal work of separation, introduced by Finnis[53] as the reversible work necessary to separate an interface into two free surfaces, does not take into account any diffusion or plasticity processes and therefore can be calculated easily by first-principles methods. A further distinction is often made between the rigid and relaxed works of separation. The former corresponds to a separation of two rigid crystal parts. In the latter, atomic relaxations are allowed to lower the total energy. In the present paper, we take the convention of stable interfaces to have positive values for the works of separation.

We determined the rigid and relaxed works of separation for all interfaces described in Figs. 1 and 2. For the rigid work of separation, the (002) interplanar spacing in all supercells was fixed to the value of interplanar spacing of ideal bulk STO and only the separation at the interface was varied to obtain the minimum energy configuration. The strain relaxation of the LAO and SRO slabs perpendicular to the interface is therefore neglected in these calculations. However, since the elastic energy contributions from the interface supercell and the free-surface supercells mutually cancel well, the results do not differ from those with the optimized tetragonal c/a ratios. For the relaxed work of separation, the stress-free LAO and SRO unit cells with optimized c/a ratios were used.

The results are summarized in Table II. We included in the table also works of separation for bulk perovskites which are equal to twice the average surface energy of AO and BO_2 terminated surface slabs. These values serve as useful references when analyzing the relative interface stabilities.

Both the rigid and relaxed works of separation show the same trend. The most stable interface in the STO/LAO system is the TiO_2-LaO terminated interface. Its work of separation lies between the values corresponding to the cleavage of the two bulk perovskites, suggesting a strong interfacial adhesion. This interface is about 25% more stable than the second defect-free interface in this system with the SrO-AlO_2 interface termination. This result differs from recent results of Gemming and Seifert[16] who obtained similar values for the two defect-free STO/LAO interfaces (quoted in parentheses in Table II). A possible origin of this discrepancy may be the use of different supercells and a different way of calculating W_{sep}. While we used the symmetrical but nonstoichiometric supercells of Fig. 1, Gemming and Seifert used a stoichiometric but asymmetrical supercell (cf. Fig. 1 in Ref. 16). Moreover, we determined W_{sep} by comparing the interface models to two surface-slab models of the same supercell dimensions with either the STO or the LAO film removed. Gemming and Seifert used an elongated asymmetrical supercell where one of the two interfaces was pulled apart while the other interface was kept fixed. In this procedure, electrical fields appear not only in the film but also in the vacuum region between the separated surfaces. Before an appropriate comparison can be made, the influence of these factors on W_{sep} needs to be analyzed. This is, however, not within the scope of the present work.

The two interfaces in the STO/LAO system containing the Ruddlesden-Popper and Magneli planar faults, respectively, exhibit almost the same works of separation. These are not only significantly lower than those for the defect-free interfaces but also lower than the work of separation of bulk STO. If present, these interfaces will therefore act as weak links in the STO/LAO heterostructures.

The results for the STO/SRO heterostructure are qualitatively similar to those for the STO/LAO heterostructure. The defect-free interfaces with the SrO-RuO_2 and TiO_2-SrO terminations have the largest works of separation and are significantly more stable than the interfaces with the Magneli- and Ruddlesden-Popper-type defects. While in the STO/LAO system, the Magneli-type planar defect was the least stable contact, in the STO/SRO system, it is the Ruddlesden-Popper-type planar defect. The Magneli-type interface in the STO/LAO system and the Ruddlesden-Popper-type interface in the STO/SRO system have similar works of separation as the same defects in pure STO.

Surprisingly, we found that the influence of relaxation on the work of separation, i.e., the difference between the energy minimum and the energy zero of the binding-energy curves (cf. Fig. 5 for two examples of these curves), is small and the difference between the rigid and relaxed works of separation is less than 0.3 J/m^2 in all cases studied. The relaxation lowers W_{sep} for all interfaces in the STO/SRO system and for the SrO-AlO_2 and the TiO_2-LaO terminations in the STO/LAO system, whereas for the SrO-LaO and TiO_2-AlO_2 interfaces with planar defects, the rigid work of separation is marginally lower than the relaxed one. In contrast, the influence of relaxation on the whole binding-energy curve is not small, and the curvature of the relaxed curves is considerably reduced (see below).

C. Interfacial structures

In order to relate the adhesion of the interfaces to their atomic structure, we analyzed the interplanar separations and local atomic relaxations of the relaxed equilibrium configurations. Results of this analysis for the STO/LAO and STO/SRO supercells are presented in Figs. 3 and 4, respectively. In these figures, we plotted the interplanar spacings along the z axis with the interface position marked as zero. Since the presence of the interface leads to a buckling of the AO and BO_2 planes due to different atomic relaxations of cations and oxygens, the interplanar distances in the cation and oxygen sublattices can be also different. The figures therefore contain three types of interplanar distances: (1) a distance between the A and B cations (marked as squares), (2) a distance between the oxygen atoms in the neighboring planes (marked as diamonds), and (3) an average interplanar distance (marked by circles). These distances are compared to reference bulk interplanar separations in ideal stress-free perovskites drawn as solid lines.

Overall, the results shown in Figs. 3 and 4 are consistent with the interfacial stabilities in Table II. The interplanar distances of the most stable, defect-free interfaces differ least from the reference bulk values throughout the supercells and the planes exhibit only very small buckling not exceeding 0.1 Å. This is in agreement with the results of Gemming and Seifert.[16] As we mentioned above, due to a common SrO sublattice in the STO/SRO heterostructure it is not possible to distinguish to which perovskite the interfacial SrO layer belongs. Based on the results shown in Fig. 4(a), we can, however, see clearly that the SrO plane behaves like belonging to STO rather than SRO since the interplanar distance to the next TiO_2 plane is the same as in bulk STO. According to this structural feature, the interface in this system is therefore located between the RuO_2 and SrO planes.

In contrast, both the interplanar separations and buckling in the interfacial region of the supercells with the stacking-fault-like interfaces differ significantly from the bulk values [see panels (c) and (d) of Fig. 3 and panels (b) and (c) of Fig. 4]. For the Ruddlesden-Popper-type interfaces, there is a significant expansion at the interface exceeding 0.7 Å, which originates most likely from a strong electrostatic repulsion between the large neighboring cations of the AO planes. The influence of the interface weakens, however, very quickly with increasing distance and already from the second plane from the interface, the interplanar spacing is again bulklike. Apart from changes of interplanar distances in the vicinity of the interface, the Magneli-type contacts exhibit the strongest buckling. The interaction between two BO_6 octahedra at the interface causes large and oppositely oriented atomic relaxations of oxygen atoms in the BO_2 planes. The opposite displacements of oxygens are indicated by the pairs of diamond symbols in Figs. 3(d) and 4(c). Similarly, as in the case of the Ruddlesden-Popper interface, this disturbance decays very

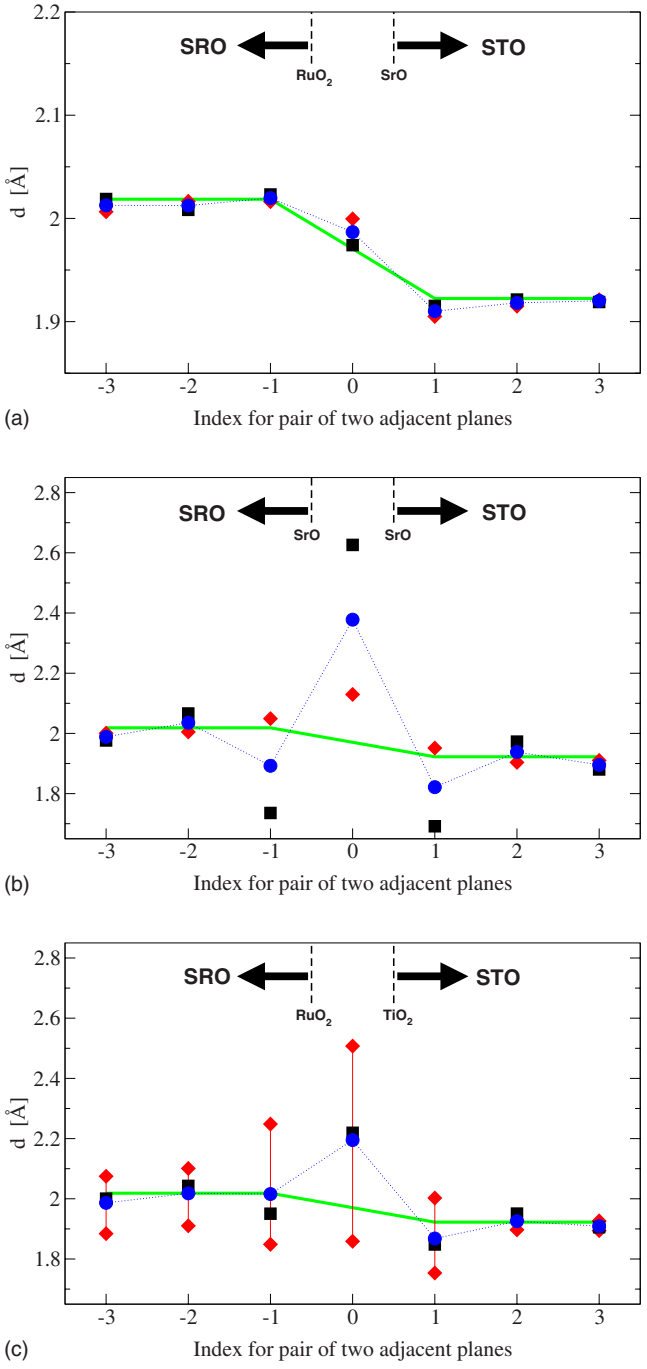

FIG. 4. (Color online) Interplanar spacings along the c axis in the four STO/SRO heterostructures. The graphs [(a)–(c)] correspond to the supercell models [(a)–(c)], respectively. Symbols are marked in the same way as in Fig. 3.

quickly with increasing distance and is localized only in a close vicinity of the interface.

In order to assess the influence of supercell size, we increased the number of layers in the perovskite slabs from 7 to 9. Additionally, in the case of the STO/LAO heterostructure, we computed the magnitude of internal relaxations calculated without the uniform background charge. We found that the results of these calculations do not noticeably differ

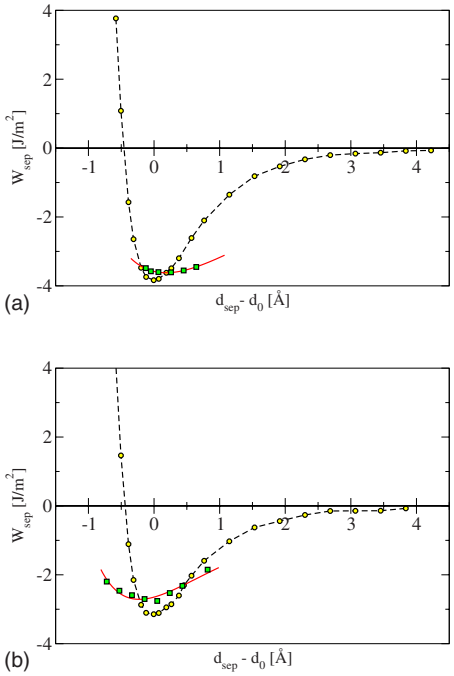

FIG. 5. (Color online) Binding-energy curves for the TiO_2-LaO interface in (a) STO/LAO and the TiO_2-SrO contact in (b) STO/SRO. The full and dashed lines correspond to the relaxed and rigid conditions, respectively.

from the results shown in Figs. 3 and 4, which were obtained with the uniform background charge.

As for the bulk SRO crystal, spin-polarized total-energy calculations for the STO/SRO supercells yielded works of separation that were different from the nonmagnetic ones by less than 0.1%. Thus, we conclude that the LDA calculations without spin polarization are a reasonable approach for heterophase systems containing magnetic SRO.

Apart from the determination of the work of separation, i.e., the minimum value of the binding energy, we also computed how the binding energy changes as the slabs are pulled apart. This information can be utilized for extracting the ideal tensile stress that is required to break the interface apart. In the case of the rigid separation, we varied only the interfacial distance while keeping the atoms at their ideal positions. In the case of relaxed separation, the same procedure was followed but the atoms were allowed to relax for each separation step. Two examples of the calculated binding-energy curves for the most stable interfaces in the STO/LAO and STO/SRO heterostructures are shown in Fig. 5. The universal binding curve[54] was fitted to the calculated DFT data. The separation d_{sep} is plotted in Fig. 5 with respect to the ideal separation d_0 based on the bulk interplanar separations in both slabs. As can be seen in Fig. 5 and as was already mentioned above, the relaxation does not change strongly the work of separation (corresponding to the minimum of the curves) but it broadens the curvature around the minimum of the binding-energy curves. This is related to a much lower ideal tensile stress needed to separate the heterostructure interface into two free surfaces.

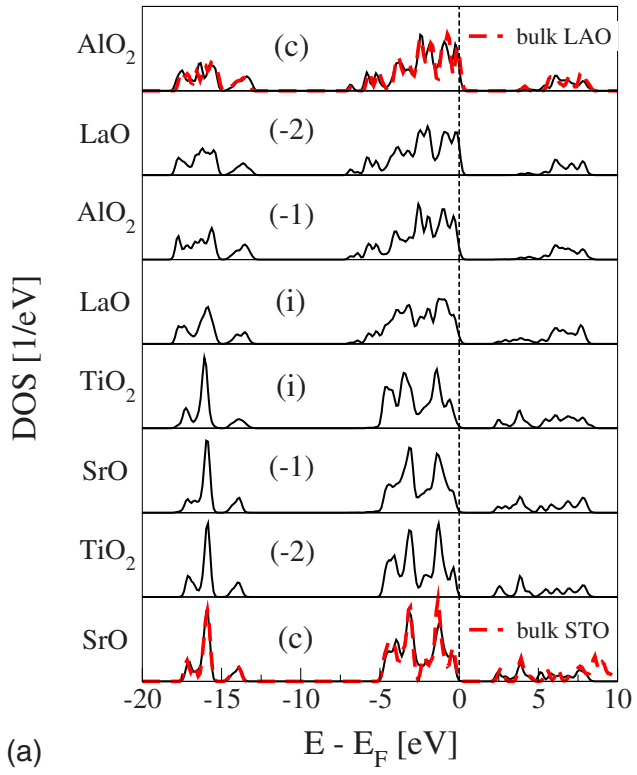

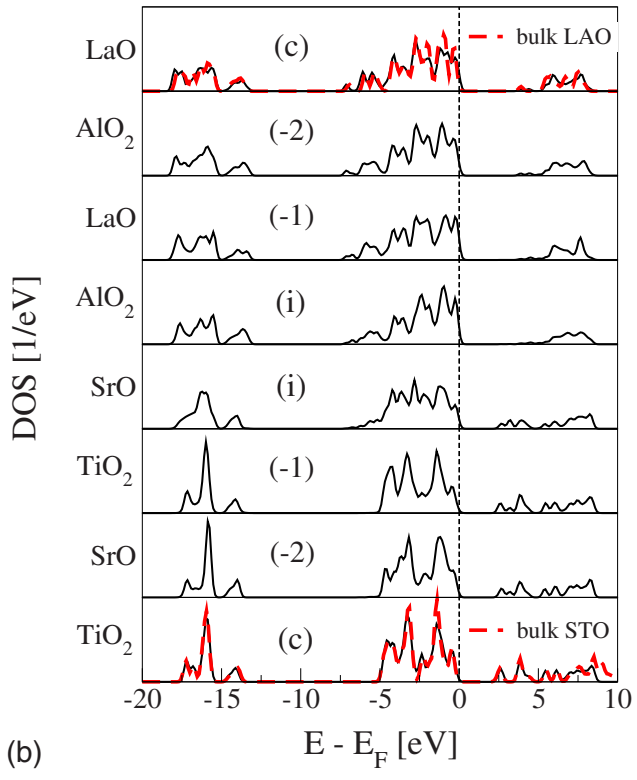

FIG. 6. (Color online) Local densities of states of the oxygen atoms in the (a) TiO_2-LaO and (b) $SrOAlO_2$ interfaces in the STO/LAO heterostructure. Dashed lines are the oxygen LDOS in bulk STO (bottom) and bulk LAO (top). Layers are labeled as (c) for central, (i) for interface, (−2) two layers away from the interface, and (−1) one layer away from the interface.

D. Electronic properties

The structurally relaxed equilibrium configurations of the interface supercells shown in Figs. 1 and 2 were used for the determination of the electron and hole Schottky barrier heights in the STO/SRO heterostructures and valence and conduction band offsets in the STO/LAO heterostructures. The Schottky barriers, valence band offsets (VBO's), and conduction band offsets (CBO's) were obtained in two different ways. First, by analyzing the local densities of states,[55] denoted further as LDOS approach, and second, by using macroscopic averages of the electrostatic potential,[56–58] denoted further as the MA approach. Both techniques have been successfully applied in band offset calculations for interfaces in various semiconductor heterostructures (see, e.g., Refs. 55, 57, and 59–61). However, due to a faster convergence of the charge density and electrostatic potential than the LDOS with distance from the interfaces, the MA technique is often assumed to provide a more reliable and accurate estimation of electrical properties than the LDOS approach with the same k-point mesh.[55] For the investigated perovskite heterostructures, we found that the LDOS method is equally accurate as the MA method.

In the LDOS method, the valence band edge values in each perovskite can be directly obtained by a single supercell calculation from the oxygen LDOS of the central layer in the slab. The central layer is the most distant layer from the interface, and for a sufficiently large supercell, it has the properties of the bulk material. A compilation of oxygen LDOS's from all (002) planes in two supercells with the most stable interfaces in the STO/LAO system are displayed in Fig. 6. The panels of the central layers (denoted as "c") contain for comparison also the LDOS of oxygen in bulk cubic STO and LAO. The close similarity between these curves confirms that the environment of the central layer in the supercells is indeed very similar to the bulk and is therefore hardly influenced by the interfaces. Note that the LDOS's in Fig. 6 are from calculations performed with compensating background charges. Without the charge compensation, the Fermi level would be shifted to the conduction band edge for LaO-terminated interfaces, and the valence band would not be completely filled for interfaces with AlO_2 terminations.

The VBO for the insulating STO/LAO heterostructure is obtained simply as the difference between the valence band edges of both materials, so that

$$E_{VBO} = E_V^{LAO} - E_V^{STO}, \tag{1}$$

where E_V are the valence band edge energies of the the two perovskites determined from the central oxygen LDOS's of the STO and LAO slabs.

The CBO is defined as the difference between the conduction band edge energies. Due to the well known inability of DFT methods to describe excited states, the magnitude of the band gap is severely underestimated (calculated values for the band gaps: $E_{gap,LDA}^{LAO}=3.6$ eV, $E_{gap,LDA}^{STO}=1.94$ eV) and cannot be used for a reliable determination of the conduction band edge. The usual way to overcome this problem is to use

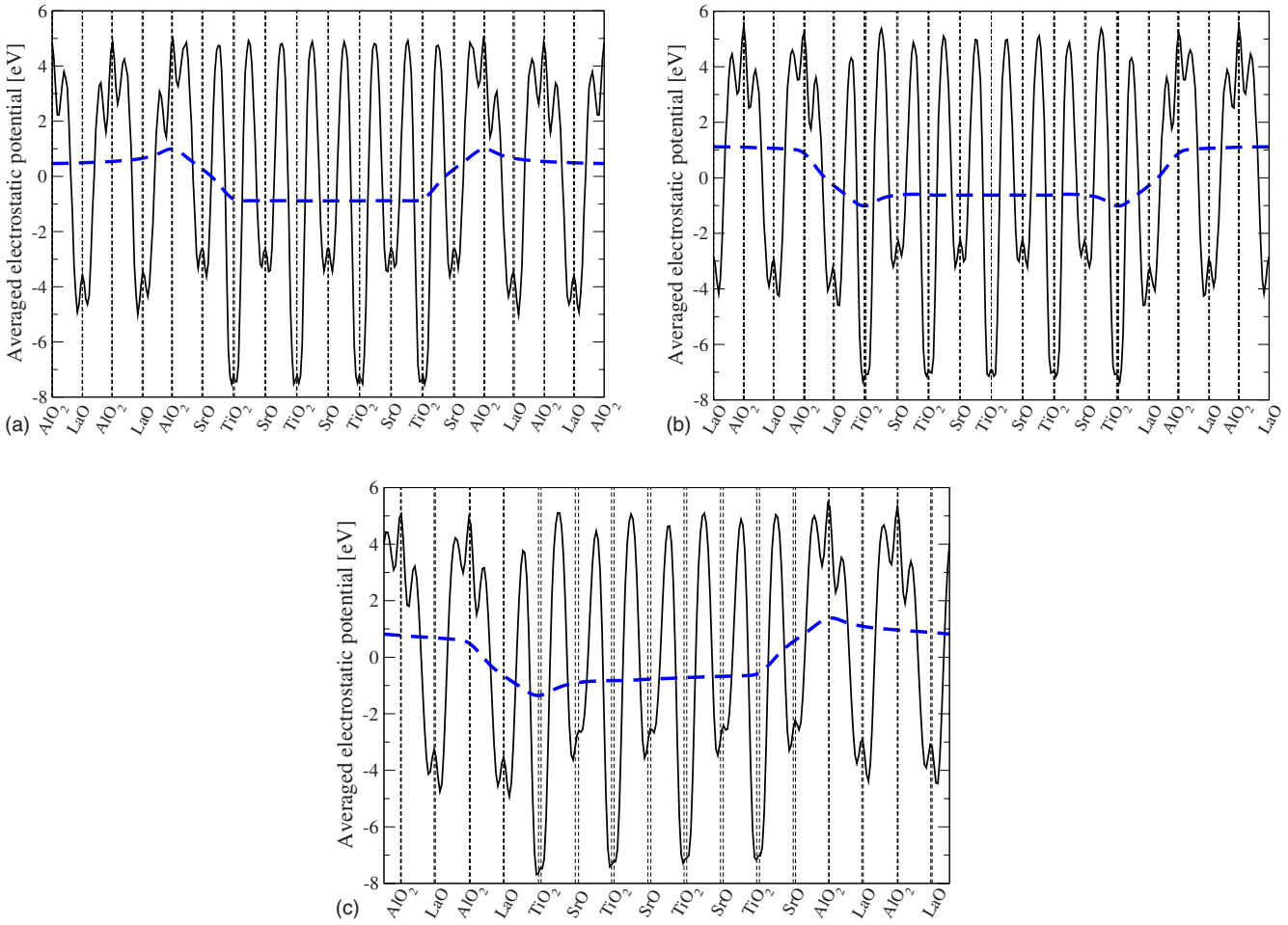

FIG. 7. (Color online) Planar average and macroscopic average of the electrostatic potential in the STO/LAO system for the symmetrical but nonstoichiometric supercells with two equivalent interfaces, (a) TiO_2-LaO and (b) SrO-AlO_2, and (c) an asymmetrical but stoichiometric supercell containing both interfaces. The dashed vertical lines mark positions of atoms in the planes.

experimental values of the band gaps.[62–64] The CBO for the STO/LAO system can then be evaluated using the simple relation

$$E_{CBO} = E_C^{LAO} - E_C^{STO}, \tag{2}$$

$$= (E_{gap}^{LAO} - E_V^{LAO}) - (E_{gap}^{STO} - E_V^{STO}), \tag{3}$$

where E_{gap}^{STO}=3.3 eV (Ref. 65) and E_{gap}^{LAO}=5.6 eV (Ref. 66) are the experimental band gaps of STO and LAO, respectively.

To estimate the influence of the finite slab thickness on the energy barriers, we carried out calculations with supercells containing both seven- and nine-layer slabs. We found that the differences between the seven- and nine-layer systems do not exceed 0.1 eV, and seven-layer systems are therefore sufficient for a reliable determination of the VBO.

The MA technique was also applied to supercells with both seven and nine layers to validate the LDOS results. Results from the seven- and nine-layer systems were again found to be very similar with a largest difference of about 0.15 eV. The variation of the planar-averaged electrostatic potential and its macroscopic average in heterostructures with the TiO_2-LaO and SrO-AlO_2 interfaces are shown in Figs. 7(a) and 7(b), respectively.

A summary of the computed band offsets in the STO/LAO heterostructures obtained by both approaches is presented in Table III. The usual convention of positive offset for an upward step when going from the left (STO) to the right slab (LAO) is used. Overall, the CBO's in all termina-

TABLE III. Valence and conduction band offsets at STO/LAO interfaces obtained by the LDOS and MA techniques from nine-layer slab calculations. The VBO's from seven-layer slab calculations are included in parentheses for comparison.

	VBO (eV)		CBO (eV)	
	LDOS	MA	LDOS	MA
SrO-AlO_2	0.10 (0.20)	0.19	2.40	2.49
TiO_2-LaO	0.39 (0.29)	0.51	2.69	2.81
SrO-LaO	−0.03 (−0.10)	0.05	2.27	2.35
TiO_2-AlO_2	0.67 (0.70)	0.74	2.97	3.04

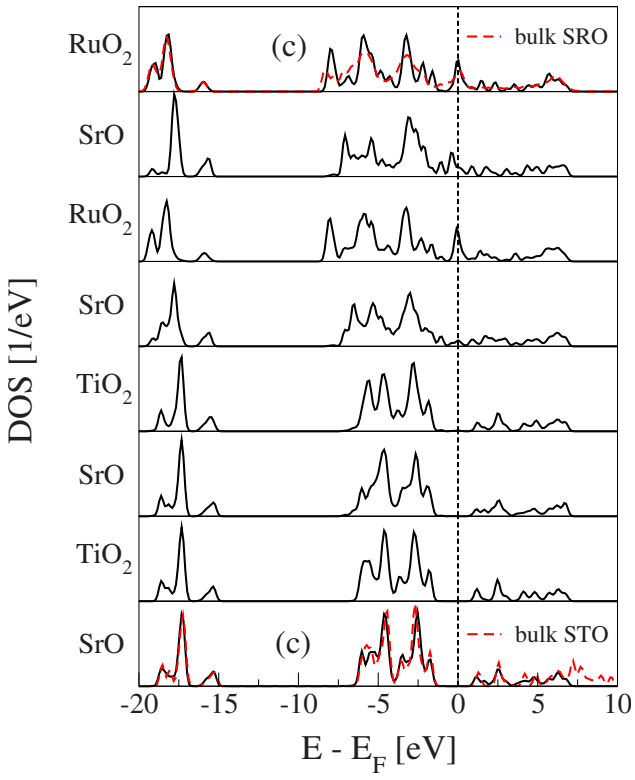

FIG. 8. (Color online) Local densities of states of the oxygen atoms for the -SrO- interface in STO/SRO.

tions are significantly larger than VBO's mainly due to the large difference of STO and LAO band gaps. For the SrO-AlO_2 and SrO-LaO interfaces, the VBO values are almost zero and increase for the TiO_2 terminated interfaces. It therefore seems that it is the STO termination at the interface rather than the regular or irregular sequence of the (002) planes that determines the magnitude of the band offsets in this system.

Finally, we consider the effect of the charge state of the system and the possible presence of net interface charges and nonzero electrical fields. In all our calculations described so far, we employed symmetrical supercells with two equivalent interfaces to avoid electrical fields. Figure 7(c) shows the averages of the electrostatic potential for an asymmetrical supercell that contains two different interfaces, TiO_2-LaO on the left and SrO-AlO_2 on the right. Even though this supercell is stoichiometric and charge neutral, large interface monopoles (local charges) are formed, causing internal electrical fields. The presence of the electrical field leads to opposite relaxations of the oxygen and cation sublattices throughout the films. As can be seen in Fig. 7(c), the relaxations (corresponding to the splitting of the vertical dashed lines that mark the layer positions) are much more pronounced in STO than in LAO. This is an expected result since STO has a much larger dielectric constant than LAO. The magnitudes of the internal electric fields in the supercell estimated from the slopes of the macroscopic potential averages are 0.26×10^9 and 0.51×10^9 V/m in the STO and LAO slabs, respectively. Interestingly, the interfacial atomic structures of the symmetrical and asymmetrical supercells do not differ significantly and the local relaxations at the interface therefore do not seem to be influenced significantly by the field.

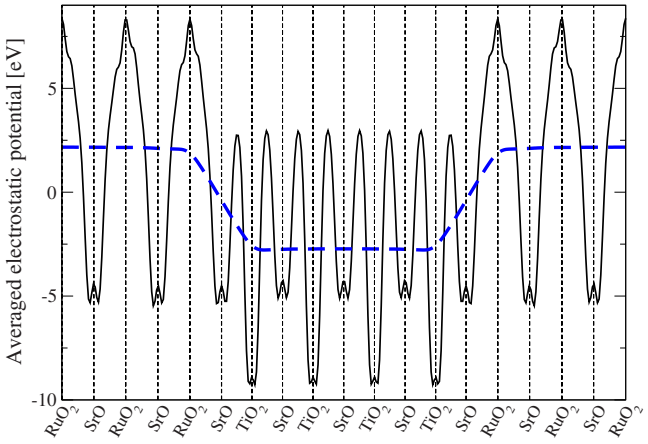

FIG. 9. (Color online) Planar average and macroscopic average of the electrostatic potential for the -SrO- interface of STO/SRO.

The plots of oxygen LDOS's for the TiO_2-SrO-RuO_2 interface (denoted only as -SrO- henceforth) in the STO/SRO system are shown in Fig. 8. The main difference between the STO/LAO and STO/SRO heterostructures is the metallic character of SRO that is responsible for metal-induced gap states (MIGS's) in the interface region. As mentioned in the previous section, based on the analysis of the interplanar separations in Fig. 4, the interfacial SrO layer belongs to STO. The electronic structure of this layer is reflected in the oxygen LDOS, which reveals that the interfacial SrO plane has features of SrO planes from both bulk STO and SRO. From the electronic structure point of view, the interface therefore cannot be identified as located precisely between the SrO plane of STO and the RuO_2 plane of SRO. Nevertheless, the spatial extent of the interface is still very narrow since the spatial range of MIGS is limited to just one layer and the LDOS converges quickly to the bulk LDOS on both sides of the interface.

For the STO/SRO heterostructure, the Schottky barriers for holes are defined as the difference between the Fermi level of SRO and the valence band edge of STO, i.e., $\phi_p = E_F^{SRO} - E_V^{STO}$. The Schottky barriers for electrons are again estimated by using the experimental band gap of STO [$E_{gap}^{STO} = 3.3$ eV (Ref. 65)] so that $\phi_n = E_{gap}^{STO} - \phi_p$. The calculated values of the Schottky barriers are summarized in Table

TABLE IV. Schottky barriers at the STO/SRO interfaces obtained by the LDOS and MA techniques.

	ϕ_p (eV)		ϕ_n (eV)	
	LDOS	MA	LDOS	MA
-SrO-	1.39 (1.36)	1.41	1.91	1.89
SrO-SrO	1.20 (1.14)	1.23	2.10	2.07
TiO_2-RuO_2	1.08 (1.03)	1.23	2.22	2.07

IV. Overall, the Schottky barriers obtained for both holes and electrons in the three different contact terminations are rather similar. With ϕ_p varying from 1.08 to 1.39 eV and ϕ_n from 1.91 to 2.22 eV, their differences are not much larger than the computational uncertainty level of about 0.1 eV.

The planar-averaged electrostatic potential and its macroscopic average for the -SrO- interface in nine-layer slabs are displayed in Fig. 9. The Schottky barriers determined by the MA method from this potential step and the bulk electronic structures of STO and SRO agree again very well with those obtained from the LDOS method.

IV. SUMMARY

We studied interfacial stabilities and electronic properties of two perovskite heterostructures using first-principles DFT calculations. The STO/LAO heterostructure was composed of two insulating perovskite oxides to mimic a substrate/film system. The STO/SRO heterostructure was chosen as a representative electrode/film system. The investigated supercells included not only interfaces with a regular perovskite stacking of alternating AO and BO_2 planes, i.e., SrO-AlO_2 and TiO_2-LaO in STO/LAO and -SrO- in STO/SRO, but also interfaces with planar stacking-fault-like defects of Ruddlesden-Popper type (SrO-LaO in STO/LAO, SrO-SrO in STO/SRO) and Magneli type (TiO_2-AlO_2 in STO/LAO, TiO_2-RuO_2 in STO/SRO). The interfacial stability was studied by calculating the rigid and relaxed works of separation and the variation of the binding energy with the interfacial separation. The calculations showed that in both heterostructures, the regular perovskite stacking is more stable than the interfaces containing planar defects.

The structurally optimized supercells of the heterostructures were used for the determination of band offsets and Schottky barriers. Depending on the interface structure, the CBO's and VBO's in the STO/LAO heterostructure vary from 2.2 to 3.0 eV and from 0 to 0.7 eV, respectively. The Schottky barriers for electrons in the STO/SRO heterostructure range from 1.9 to 2.2 eV and for holes from 1.1 to 1.4 eV. Results obtained by the macroscopic averaging approach and by the LDOS analysis are consistent within about 0.15 eV. For practical application, we can conclude that the magnitudes of the Schottky barriers and CBO's for electrons in the investigated heterostructures are sufficiently large and not influenced significantly by the interfacial termination.

ACKNOWLEDGMENTS

Financial support for this work was provided by the German Research Foundation (DFG) through the project El 155/17-1 in the priority program 1157 "Integrated electroceramic functional structures" and by the European Commission through Contract NMP3-CT-2005-013862 (INCEMS). The authors thank N. Benedek for valuable discussions.

[1] N. Setter and R. Waser, Acta Mater. **48**, 151 (2000).
[2] M. Dawber, K. M. Rabe, and J. F. Scott, Rev. Mod. Phys. **77**, 1083 (2005).
[3] A. I. Kingon, J. P. Maria, and S. K. Streiffer, Nature (London) **406**, 1032 (2000).
[4] D. E. Kotecki *et al.*, IBM J. Res. Dev. **43**, 367 (1999).
[5] J. Robertson, Rep. Prog. Phys. **69**, 327 (2006).
[6] O. Auciello, J. Appl. Phys. **100**, 051614 (2006).
[7] A. Ohtomo and H. Y. Hwang, Nature (London) **427**, 423 (2004).
[8] N. Nakagawa, H. Y. Hwang, and D. A. Muller, Nat. Mater. **5**, 204 (2006).
[9] M. Huijben, G. Rijnders, D. Blank, S. Bals, S. Aert, J. Verbeeck, G. Tendeloo, A. Brinkman, and H. Hilgenkamp, Nat. Mater. **5**, 556 (2006).
[10] S. Thiel, G. Hammerl, A. Schmehl, C. Schneider, and J. Mannhart, Science **313**, 1942 (2006).
[11] W. Siemons, G. Koster, H. Yamamoto, W. A. Harrison, G. Lucovsky, T. H. Geballe, D. H. A. Blank, and M. R. Beasley, Phys. Rev. Lett. **98**, 196802 (2007).
[12] A. Kalabukhov, R. Gunnarsson, J. Börjesson, E. Olsson, T. Claeson, and D. Winkler, Phys. Rev. B **75**, 121404(R) (2007).
[13] A. Brinkman, M. Huijben, M. van Zalk, J. Huijben, U. Zeitler, J. Maan, W. van der Wiel, G. Rijnders, D. Blank, and H. Hilgenkamp, Nat. Mater. **6**, 493 (2007).
[14] J. Maurice, C. Carrétéro, M. Casanove, K. Bouzehouane, S. Guyard, É. Larquet, and J. Contour, Phys. Status Solidi A **203**, 2209 (2006).
[15] Y. L. Qin, C. L. Jia, K. Urban, J. H. Hao, and X. X. Xi, J. Mater. Res. **17**, 3117 (2002).
[16] S. Gemming and G. Seifert, Acta Mater. **54**, 4299 (2006).
[17] R. Pentcheva and W. E. Pickett, Phys. Rev. B **74**, 035112 (2006).
[18] M. S. Park, S. H. Rhim, and A. J. Freeman, Phys. Rev. B **74**, 205416 (2006).
[19] C. L. Chen, Y. Cao, Z. J. Huang, Q. D. Jiang, Z. Zhang, Y. Y. Sun, W. N. Kang, L. M. Dezaneti, W. K. Chu, and C. W. Chu, Appl. Phys. Lett. **71**, 1047 (1997).
[20] J. C. Jiang, W. Tian, X. Q. Pan, Q. Gan, and C. B. Eom, Appl. Phys. Lett. **72**, 2963 (1998).
[21] R. A. Rao, Q. Gan, and C. B. Eom, Appl. Phys. Lett. **71**, 1171 (1997).
[22] C. B. Eom, R. J. Cava, R. M. Fleming, J. M. Phillips, R. B. van Dover, J. H. Marshall, J. W. P. Hsu, J. J. Krajewski, and W. F. Peck, Jr., Science **258**, 1766 (1992).
[23] N. Okuda, K. Saito, and H. Funakubo, Jpn. J. Appl. Phys., Part 1 **39**, 572 (2000).
[24] S. Wu, C. L. Jia, K. Urban, J. H. Hao, and X. X. Xi, J. Mater. Res. **16**, 3443 (2001).
[25] K. Takahashi, T. Oikawa, K. Saito, S. Kaneko, H. Fujisawa, M. Shimizu, and H. Funakubo, Jpn. J. Appl. Phys., Part 1 **41**, 5376 (2002).
[26] C. Jia, J. Rodriguez Contreras, J. Schubert, M. Lentzen, U. Poppe, H. Kohlstedt, K. Urban, and R. Waser, J. Cryst. Growth **247**, 381 (2003).
[27] S. Oh and C. Park, J. Mater. Res. **21**, 1550 (2006).

[28] P. Hohenberg and W. Kohn, Phys. Rev. **136**, B864 (1964).
[29] W. Kohn and L. J. Sham, Phys. Rev. **140**, A113 (1965).
[30] C. Elsässer, N. Takeuchi, K. M. Ho, C. T. Chan, P. Braun, and M. Fähnle, J. Phys.: Condens. Matter **2**, 4371 (1990).
[31] K. M. Ho, C. Elsässer, C. T. Chan, and M. Fähnle, J. Phys.: Condens. Matter **4**, 5189 (1992).
[32] B. Meyer, K. Hummler, C. Elsässer, and M. Fähnle, J. Phys.: Condens. Matter **7**, 9201 (1995).
[33] F. Lechermann, F. Welsch, C. Elsässer, C. Ederer, M. Fähnle, J. M. Sanchez, and B. Meyer, Phys. Rev. B **65**, 132104 (2002).
[34] B. Meyer, C. Elsässer, F. Lechermann, and M. Fähnle, FORTRAN90, program for mixed-basis pseudopotential calculations for crystals, Max-Planck-Institut für Metallforschung Stuttgart.
[35] D. M. Ceperley and B. J. Alder, Phys. Rev. Lett. **45**, 566 (1980).
[36] J. P. Perdew and A. Zunger, Phys. Rev. B **23**, 5048 (1981).
[37] D. Vanderbilt, Phys. Rev. B **32**, 8412 (1985).
[38] H. J. Monkhorst and J. D. Pack, Phys. Rev. B **13**, 5188 (1976).
[39] K. Nassau and A. E. Miller, J. Cryst. Growth **91**, 373 (1988).
[40] S. Geller and V. B. Bala, Acta Crystallogr. **9**, 1019 (1956).
[41] C. W. Jones, P. D. Battle, P. Lightfoot, and W. T. A. Harrison, Acta Crystallogr., Sect. C: Cryst. Struct. Commun. **C45**, 365 (1989).
[42] T. Ochs, S. Köstlmeier, and C. Elsässer, Integr. Ferroelectr. **32**, 267 (2001).
[43] S. N. Ruddlesden and P. Popper, Acta Crystallogr. **11**, 54 (1958).
[44] K. Szot and W. Speier, Phys. Rev. B **60**, 5909 (1999).
[45] T. Suzuki and M. Fujimoto, J. Appl. Phys. **89**, 5622 (2001).
[46] S. Andersson, B. Collen, U. Kuylenstierna, and A. Magneli, Acta Chem. Scand. (1947-1973) **11**, 1641 (1957).
[47] F. Bernardini and V. Fiorentini, Phys. Rev. B **57**, R9427 (1998).
[48] D. Cociorva, W. Aulbur, and J. Wilkins, Solid State Commun. **124**, 63 (2002).
[49] D. J. Singh, J. Appl. Phys. **79**, 4818 (1996).
[50] S. Kimura, J. Yamauchi, M. Tsukada, and S. Watanabe, Phys. Rev. B **51**, 11049 (1995).
[51] G. Santi and T. Jarlborg, J. Phys.: Condens. Matter **9**, 9563 (1997).
[52] A. Callaghan, C. W. Moeller, and R. Ward, Inorg. Chem. **5**, 1572 (1966).
[53] M. W. Finnis, J. Phys.: Condens. Matter **8**, 5811 (1996).
[54] J. H. Rose, J. R. Smith, and J. Ferrante, Phys. Rev. B **28**, 1835 (1983).
[55] M. Peressi, N. Binggeli, and A. Baldereschi, J. Phys. D **31**, 1273 (1998).
[56] A. Baldereschi, S. Baroni, and R. Resta, Phys. Rev. Lett. **61**, 734 (1988).
[57] L. Colombo, R. Resta, and S. Baroni, Phys. Rev. B **44**, 5572 (1991).
[58] J. Junquera, M. Cohen, and K. Rabe, J. Phys.: Condens. Matter **19**, 213203 (2007).
[59] J. Junquera, M. Zimmer, P. Ordejon, and P. Ghosez, Phys. Rev. B **67**, 155327 (2003).
[60] X. Zhang, A. A. Demkov, H. Li, X. Hu, Y. Wei, and J. Kulik, Phys. Rev. B **68**, 125323 (2003).
[61] A. A. Knizhnik, I. M. Iskandarova, A. A. Bagatur'yants, B. V. Potapkin, L. R. C. Fonseca, and A. Korkin, Phys. Rev. B **72**, 235329 (2005).
[62] J. Robertson and C. W. Chen, Appl. Phys. Lett. **74**, 1168 (1999).
[63] C. Van de Walle and J. Neugebauer, J. Appl. Phys. **95**, 3851 (2004).
[64] S. Zhang, J. Phys.: Condens. Matter **14**, R881 (2002).
[65] K. van Benthem, C. Elsässer, and R. H. French, J. Appl. Phys. **90**, 6156 (2001).
[66] S. G. Lim, S. Kriventsov, T. N. Jackson, J. H. Haeni, D. G. Schlom, A. M. Balbashov, R. Uecker, P. Reiche, J. L. Freeouf, and G. Lucovsky, J. Appl. Phys. **91**, 4500 (2002).